Open Archive Toulouse Archive Ouverte

OATAO is an open access repository that collects the work of Toulouse researchers and makes it freely available over the web where possible

This is an author's version published in: http://oatao.univ-toulouse.fr/24156

Techno-economical optimization of wind power production including lithium and/or hydrogen sizing in the context of the day ahead market in island grids

David Hernández-Torres, Christophe Turpin, Xavier Roboam*, Bruno Sareni

Laboratoire Plasma et Conversion d'Energie (LAPLACE), UMR5213-CNRS-INPT-UPS, Toulouse, France

Abstract

In this article an optimal storage sizing based on technical and economical modeling is presented. A focus is made on wind power producers participating in day-ahead markets for island networks and energy storage using Li-Ion and H2/O2 batteries. The modeling approach is based on power flow models and detailed optimization-oriented techniques. An importance is given to the storage device ageing effects on the overall hybrid system levelized cost of the energy. The results are presented for the special case of renewable power integration in the French islands networks. The analysis obtained after the results shows the importance of this type of modeling tool for decision making during the initial conceptual design level.

1. Introduction

The massive integration of renewable energy sources (RES) in island networks is of great concern because of the absence of extended, robust and interconnected electric infrastructures. Mature and well established technologies, such as wind and solar power, are intermittent by nature, thus limiting the amount of installed power available from these sources in order to avoid stability problems. Energy storage systems (ESS) are a solution to cope with the intermittent character of renewable sources. They are used to efficiently smooth power output and to store exceeding or failing production. In the context of French island networks with high penetration rates of renewable energy already installed (e.g. Réunion and Guadeloupe islands), a limitation of 30% in renewable penetration rate has been imposed in order to preserve the electrical grid stability. Storage devices with power management could then be used to increase the saturated renewable penetration ratio in these sites.

---

* Corresponding author.
E-mail addresses: dhernandez@laplace.univ-tlse.fr (D. Hernández-Torres), turpin@laplace.univ-tlse.fr (C. Turpin), roboam@laplace.univ-tlse.fr (X. Roboam), sareni@laplace.univ-tlse.fr (B. Sareni).

In this kind of system, the installation should be capable of managing in real-time, the produced power from the sources and the storage devices, in order to propose a good quality power delivery service. Under the condition of a storage device installation, the wind power producers are allowed to participate in forward markets, particularly in the day-ahead market, where the majority of today's agreements of power delivery are made [5]. The energy management system of the hybrid plant should be able to guarantee the commitment imposed by the day-ahead planning in order to avoid penalties from the grid operator. This kind of restrictions imposes that the energy management strategies (EMSs) should be precise, but also that the storage system should be properly sized to guarantee the power commitment under uncertain stochastic power production from renewable sources. The problem of EMSs design has been broadly studied in the literature. The impact of optimal EMSs for maximizing the profit of a wind power producer is well presented in [5]. Other interesting optimal EMSs are presented in [24,23,16,9]. Some practical and efficient rule-based/heuristic EMSs with RES are also given in [15,14,4,8]. Intermediate studies considering both optimal control and sizing for RES integration to power networks are presented in [6] using linear programming and model predictive control and in [12] using dynamic programming and optimal control.

A similar modeling philosophy is used in [17] or even in [10]. However, the tools proposed in these works are proprietary and often not modifiable (new EMSs techniques or even different grid ancillary services are hard to implement). Some original and efficient heuristic EMSs for several RES and ESS types can be found in [14,4].

Other interesting optimal sizing approaches are developed in the literature, using constrained optimization on a simplified techno-economical model in [18], or using optimal cost minimization with a battery ageing model in [25]. Optimal sizing is also studied in electricity markets using special bidding planning strategies in [19] and with a risk hedging against penalties strategy in [21]. ESS sizing is also proposed based on the forecast data statistical information in [3]. The impact on storage sizing of the day-ahead forecast is presented in [11].

This article is focused on the modeling and optimal sizing of a system with ESS associated with RES using a techno-economic perspective. A simulation and optimization tool has been developed at LAPLACE laboratory in Toulouse to study this type of system. The modeling approach is oriented towards an optimal sizing of storage devices. It is then important to consider models that are valid in the scale of the system life span (i.e. several years). Following this modeling approach, a focus is given in this article to heuristic EMSs techniques. The main contribution of this article is the integration of an optimal sizing methodology for long simulation horizons, on the scale of the system life span, including the nonlinearities of the ESS by considering detailed optimization-oriented models of the ESS. Ageing and degradation models of the ESS are of special interest in this article.

This article is divided in three main sections. In the two first sections the system modeling and the energy management strategies are described. The last section is devoted to the presentation of the obtained results.

2. System modeling

In this section several power flow models are presented including the model of a wind farm production, a Li-Ion battery and the economical model considered in this article. As a general rule the powers are supposed constant during a time step Δt ($\Delta t = 10$ min).

2.1. Wind farm model

The model of a wind farm production considered in this article is a simplified computation of the output power in kW as a function of the wind speed in m/s. The model is based on the power curve of the chosen wind turbine and is basically a power flow model that considers bulk production losses and potential energy variation with the height of the turbine.

In this article we will focus on a variable speed turbine, rated 2 MW, with a 80 m diameter.

In this model the real output power is computed by a correction of the power curve output power by subtraction of the bulk productions losses:

$$\tilde{P}_{WT} = (1 - losses) \times P_{WT} \tag{1}$$

where $\tilde{P}_{WT}$ and P_{WT} are the wind farm output power with and without losses and the total $losses$ are estimated at 12.9% representative of wake effect, availability, electrical efficiency, environmental factors losses. These production losses are based on real data provided by our industrial partner, which is a major and experienced player among wind power producers in France.
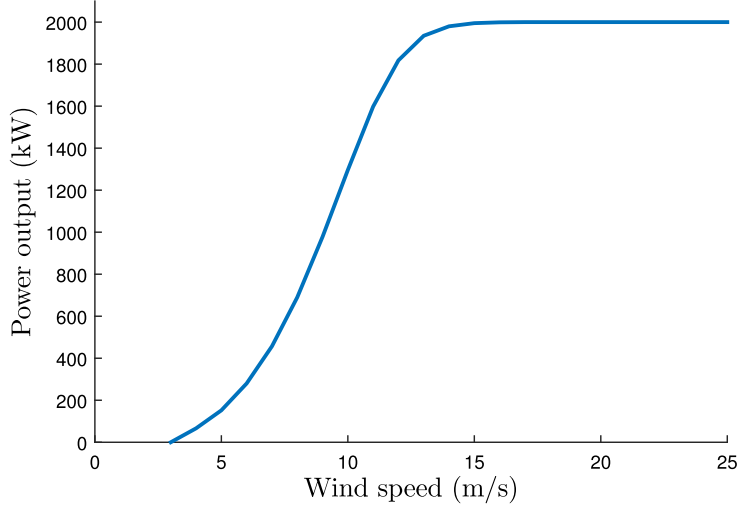
Fig. 1. Power curve for the 2 MW wind turbine.

A final correction to the output power consists in the potential energy variation with the height of the turbine. It is the impact of the difference height between wind measurements and the actual turbine hub. The wind shear effect may be estimated using the following algorithmic law:

$$\frac{U_{hub}}{V_{meas}} = \frac{\ln(z_{hub}/z_0)}{\ln(z_{meas}/z_0)} \tag{2}$$

where U and z are respectively the wind speed and height, subscripts hub and $meas$ denote the turbine hub and the wind measurement and z_0 is a height reference corresponding to the terrain roughness index. For a rough pasture terrain, $z_0 = 0.01$ m.

Wind measurements and forecast data used in this article were provided for a site in Guadeloupe island. The wind farm is composed of four 2 MW turbines, for a total installed power of 8 MW. The annual energy output is expected to be around 16 GWh, therefore the load factor is assessed around 23%. The turbine power curve and a one week sample of wind power production and forecast are presented in Figs. 1 and 2 respectively.

A synthetic data generation methodology has been developed to fill for a complete year of wind measurements and forecast. This method can also be used to generate the input vectors needed for the system simulation at the scale of the system life span (several years). We use the phase-randomizing method proposed in [22].

The method is an extension of the multi-variable case of an algorithm based on the Fourier transform to generate data to replace a limited time horizon data set. The new generated data set is not only representative of the correlation between the variables (wind measurement and forecast in this case), but also of the correlation between time steps in the time series. For the mono-variable case, two methods are normally used to tackle this kind of problem. In the first method, a model of the original data set is directly identified, using an ARMA model. In the second, the Fourier transform is applied to the data set, a random variable is introduced to the phases and the inverse transform is computed.

For a time series $x(t)$, composed of N values taken at a regular time step $t = t_0, t_1, \ldots, t_{N-1} = 0, \Delta t, \ldots, (N-1)\Delta t$, the Fourier transform is obtained by applying the $\mathcal{F}$ operator:

$$X(f) = \mathcal{F}\{x(t)\} = \sum_{n=0}^{N-1} x(t_n)e^{2\pi i f n \Delta t} \tag{3}$$

This complex value may be rewritten as:
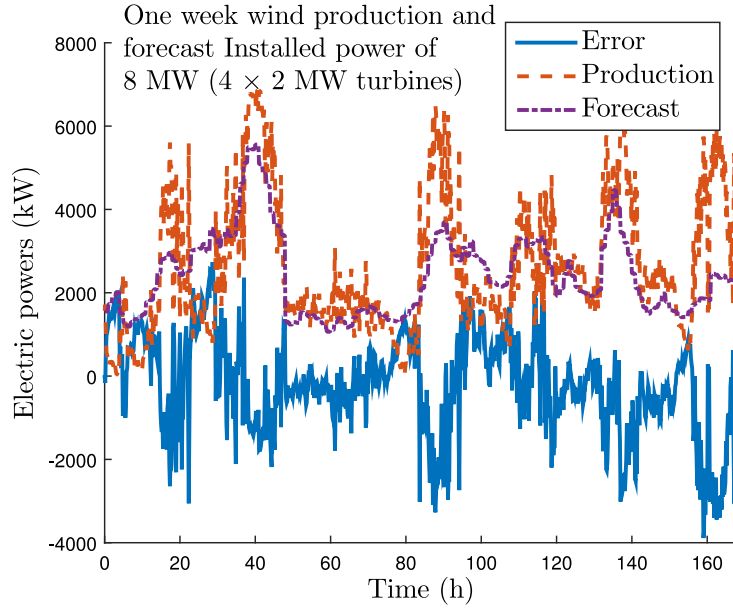
$$X(f) = A(f)e^{i\phi(f)} \tag{4}$$

Fig. 2. One week sample of wind production and forecast.

where $A(f)$ is the amplitude and $\phi(f)$ is the phase. A phase-randomizing Fourier transform is built by introducing a random rotation Φ to the phase ϕ, this is:

$$\tilde{X}(f) = A(f)e^{i[\phi(f)+\Phi(f)]} \tag{5}$$

Applying the inverse transform the new data set is obtained:

$$\tilde{x}(t) = \mathcal{F}^{-1}\{\tilde{X}(f)\} = \mathcal{F}^{-1}\{X(f)e^{i\varphi(f)}\} \tag{6}$$

By mathematical principle, the time series $\tilde{x}(t)$ will have the same spectral power density and the same autocorrelation as $x(t)$.

For the multi-variable case, let us suppose that we have m simultaneously measured variables $x_1(t), x_2(t), \ldots, x_m(t)$ with $X_1(t), X_2(t), \ldots, X_m(t)$ their Fourier transform. The inter-correlation between the jth and kth variables is defined by:

$$C_{jk}(\tau) = \langle x_j(\tau)x_k(t-\tau) \rangle \tag{7}$$

The Fourier transform of this inter-correlation gives us the inter-spectrum between variables:

$$X_j^*(f)X_k(f) = A_j(f)A_k(f)e^{i[\phi_k(f)-\phi_j(f)]} \tag{8}$$

Here $X_j^*(f)X_k(f)$ must be fixed for each pair (j, k), for auto-correlations and inter-correlations to be guaranteed. As we want to add a phase to the equation, a random sequence $\varphi(f)$ must be added to $\phi(f)$ for each j. This is:

$$\tilde{x}_j(t) = \mathcal{F}^{-1}\{X_j(f)e^{i\varphi(f)}\} \tag{9}$$

2.2. Li-Ion battery model

A classic optimization-oriented model to represent the Li-Ion battery is limited to the definition of a charge/ discharge efficiency. A presentation of this type of model is given in detail in [1].

This model has been widely used in optimization-oriented modeling approaches. Despite the simplicity and fast simulation times offered by this type of model, several problems arise with this methodology. A first problem relies on
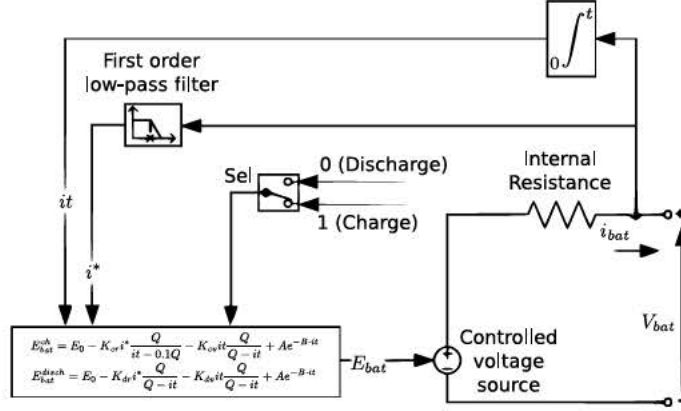
Fig. 3. Electrical-equivalent battery model.

the fact that the battery efficiency is not a typical parameter given in battery data-sheets. Moreover, in real applications, the battery voltage is monitored under operating conditions at all times. Most importantly, a dissociation of voltage and current in the model will be useful for the implementation of a precise model of the battery ageing considering degradation parameters. For these reasons, an interest is given to models separating voltage/current variables. We will focus on the model proposed in [28].

This is a dynamical model of the battery based on the following equations in charge/discharge conditions, with a clarification of variables homogeneity compared to the notation used in [28]:

$$V_{bat}^{ch} = E_0 - R_{int} \cdot i_{bat} - K_{cr}i^* \frac{Q}{it - 0.1Q} - K_{cv}it \frac{Q}{Q - it} + Ae^{-B \cdot it} \tag{10}$$

$$V_{bat}^{disch} = E_0 - R_{int} \cdot i_{bat} - K_{dr}i^* \frac{Q}{Q - it} - K_{dv}it \frac{Q}{Q - it} + Ae^{-B \cdot it} \tag{11}$$

where E_0 denotes the constant battery voltage in V, R_{int} the internal battery resistance in Ω, K_{cr}, K_{dr} the polarization resistances in charge/discharge in Ω, K_{cv}, K_{dv} the polarization constants in charge/discharge V/Ah, Q the battery capacity in Ah, A the amplitude of the exponential zone in V, B the inverse time constant of the exponential zone in Ah^{-1}, $it = \int i_{bat}dt$ the actual battery charge in Ah and i^* the low frequency component of current i_{bat} ($i^* = i_{bat}/(1 + s\tau)$ with τ the filter time constant). The electrical-equivalent model slightly modified from [28], is presented in Fig. 3. We consider a simplification with $K = K_{cr} = K_{cv} = K_{dr} = K_{dv}$. After a parameter fitting on data-sheet V–I curves for a SAFT VL41M Li-Ion cell, the following parameters are obtained: $E_0 = 3.24$ V; $A = 0.75$ V; $B = 0.03$ Ah^{-1}; $K = 1.04 \times 10^{-4}$ V/Ah; $R_{int} = 1.97 \times 10^{-3} \Omega$. The V–I curves for several discharge currents for the SAFT VL41M cell and the identified model are presented in Fig. 4.

Another simplification for our application is to consider the current i^* in a steady state condition, i.e. $i^* = i_{bat}$. The discrete implementation of the actual battery charge it is given by:

$$it[k] = it[k - 1] + i_{bat}[k]\Delta t \tag{12}$$

where Δt is the time step of the simulation. With the actual charge it, the state of charge is estimated by the equation:

$$SOC[k] = SOC[k - 1] - \frac{it[k]}{Q}\Delta t \tag{13}$$

A modification using linear interpolation can be added to this model to correct the energy balance of the charged/discharged energies for the special cases of the SOC saturating at its upper or lower limits. This correction is necessary when using large simulation time steps (typically greater than $\Delta t > 1$ min) [13].

Ageing model of the Li-Ion battery

The ageing model used in this work is a battery parameter degradation model based on the accumulation of the energy exchanged by the battery. With this approach, the system degradation after usage has an effect on both
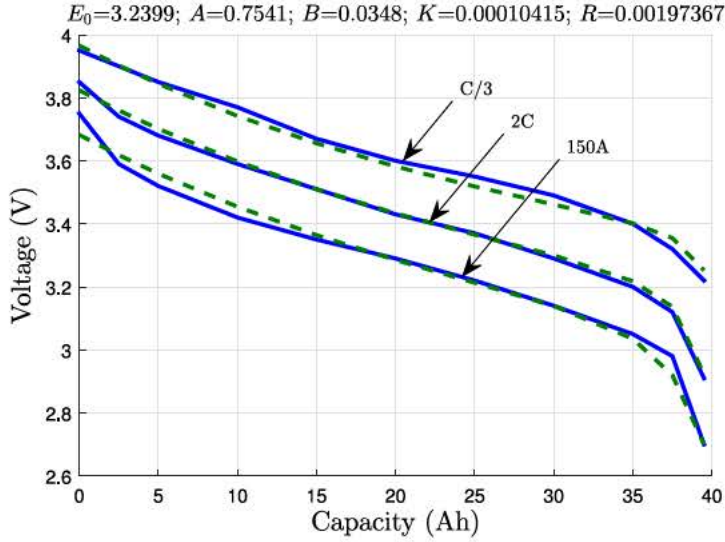
$E_0=3.2399$; $A=0.7541$; $B=0.0348$; $K=0.00010415$; $R=0.00197367$

Fig. 4. Discharge V–I curves for SAFT VL41M cell.

technical and economical variables in our model. This type of model expresses the state of health as a function of the accumulated energy exchanged by the battery at each time step and the total energy that the battery can exchange during its life span. This maximum energy quantity can be computed using the cycle to failure curve from the battery data-sheet [26]. The maximum exchangeable energy $E_{exch_{max}}$ is calculated as a function of the maximum depth of discharge and the total number of cycles (obtained from the cycle to failure curve) as follows:

$$E_{exch_{max}} = 2 \times N_{cyclesMax}(DOD_{max})DOD_{max}E_{nom} \tag{14}$$

where E_{nom} is the nominal healthy battery energy in kWh. The maximum depth of discharge can be fixed with min/max limits on the battery SOC. The state of health of the battery is computed by:

$$SOH[k] = SOH[k-1] - \frac{|E_{exch}[k]|}{E_{exch_{max}}} \tag{15}$$

In this article a battery container is defined as 2×10 parallel and 7×29 series VL41M cells. For this battery size and a limitation $DOD_{max} = 60\%$, the maximum lifetime exchangeable energy is 4900 MWh approximatively. This approach has the advantage of being compact and compatible with an optimization-oriented modeling as the SOH may be computed at each step time. It is also a computation method where ageing parameters will have a direct impact on both technical and economical indicators. The battery end of life (EOL with $SOH = 0\%$) is obtained when the cumulated exchanged energy E_{exch} reaches the maximum exchangeable energy value $E_{exch_{max}}$.

The degraded parameters are the battery capacity Q and the internal resistance R_{int}. We suppose a linear degradation of these parameters as a function of the SOH. According to the data-sheet data for a SAFT VL41M cells, the battery end of life (EOL) is considered when the capacity falls beyond 70% of the nominal capacity.

$$Q_{EOL}^{deg} = 70\%Q^{nom} \tag{16}$$

Supposing a linear correspondence with the SOH we obtain:

$$Q^{deg} = Q^{nom} \times \left(Q_{EOL}^{deg}/Q^{nom} + \left(1 - Q_{EOL}^{deg}/Q^{nom}\right)SOH \right) \tag{17}$$

For a capacity fading of 70% we suppose a resistance rise of 170% at the battery end of life.

$$R_{intEOL}^{deg} = 170\%R_{int}^{nom} \tag{18}$$

For a linear correspondence with the SOH we obtain:

$$R_{int}^{deg} = R_{int}^{nom} \times \left(1 + \left(R_{intEOL}^{deg}/R_{int}^{nom} - 1^{deg}\right)(1 - SOH)\right) \tag{19}$$
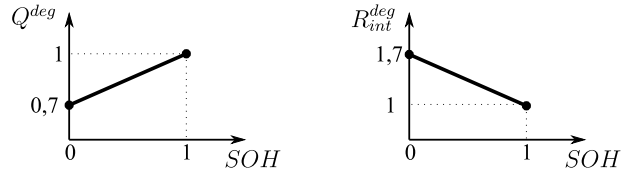
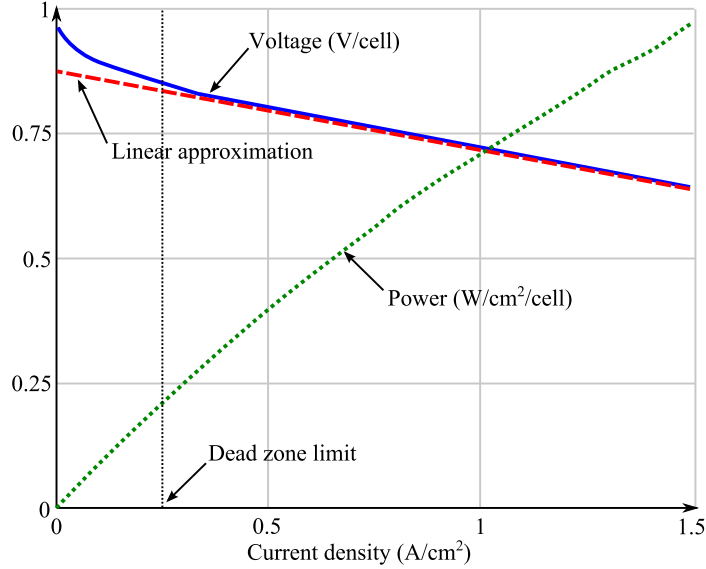**Fig. 5.** Linear degraded parameters.

Fig. 6. Linear approximation on the FC polarization curve.

These parameters are directly introduced in Eqs. (10) and (11). Fig. 5 shows an outline of the linear parameter degradation characteristics.

2.3. H2/O2 battery model

The model presented in this section describes the behavior of a H2/O2 battery from an energetic perspective. The H2/O2 energy storage system is composed of an electrolyzer, a fuel cell and H2 and O2 tanks. The model presented in this article is derived from a knowledge model developed in LAPLACE laboratory and partially presented in [7].

For the fuel cell (FC) model, we suppose a linear behavior on the V–I polarization curve, accepting an important modeling error for current densities between 0.05 and 0.25 A/cm2. This linear approximation is graphically described in Fig. 6. However, this assumption is acceptable since a dead band is defined at low current densities for security reasons (crossover) and to guarantee the auxiliary systems energy consumption (an autonomous FC system is considered). This means that there is a minimum power P_{minaux} from which the FC begins delivering effective power.

The net output power of the FC P_{outFC} is defined as the power delivered by the FC after deduction of auxiliary systems consumption. The auxiliary systems power consumption is defined by:

$$P_{aux} = P_{minaux} + k P_{stack} \tag{20}$$

where k is the fraction of the power consumed by the auxiliary systems in terms of the nominal FC stack power. The net output power of the FC is given by:
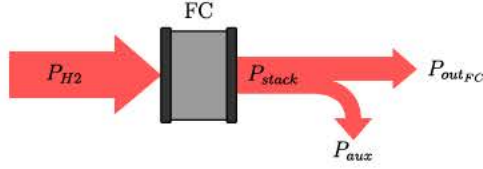
$$P_{outFC} = P_{stack} - P_{aux} \tag{21}$$

Fig. 7. Input/output FC power flow.

Then, the power at the stack output is computed by:

$$P_{stack} = \frac{P_{out\,FC} + P_{minaux}}{1 + k} \tag{22}$$

An input/output FC power flow diagram is presented in Fig. 7.

The cell power density in W/cm^2 is defined by:

$$p_{stack} = \frac{P_{stack}}{S_{cell}\,N_{cell}} \tag{23}$$

where S_{cell} is the cell surface in cm^2 and N_{cell} is the number of series connected cells. With the terminal voltage of the stack $V_{FC} = E_{FC} - R_{FC}i$ and the power density $p_{FC} = V_{FC}i = (E_{FC} - R_{FC}i)\,i$, the following polynomial is obtained:

$$i^2 - \frac{E_{FC}}{R_{FC}}i - \frac{p_{FC}}{R_{FC}} = 0 \tag{24}$$

Solving this quadratic equation for the current density i in A/cm^2 is given by:

$$i = \frac{1}{2}\left[\frac{E_{FC}}{R_{FC}} - \sqrt{\frac{E_{FC}^2}{R_{FC}^2} - 4\frac{p_{FC}}{R_{FC}}} \right] \tag{25}$$

With a molar flow $J_i = \frac{I}{2F} = \frac{i S_{cell}}{2F} = \frac{dn}{dt}$, we obtain:

$$\Delta n = \frac{i\,S_{cell}}{2F}3600\Delta t \tag{26}$$

where n is the number of H2 moles consumed in the energy conversion during on time step Δt and $F = 96{,}485$ is the Faraday constant in C/mol. Substituting (25) in (26) gives:

$$\Delta n_{stack} = \frac{3600\Delta t}{4F}\left[\frac{E_{FC}}{R_{FC}} - \sqrt{\frac{E_{FC}^2}{R_{FC}^2} - 4\frac{P_{stack}}{R_{FC}S_{cell}N_{cell}}} \right] S_{cell}N_{cell} \tag{27}$$

We follow the same approach for the electrolyzer (ELYZ) model. However this time the power consumed by the auxiliary systems is obtained from the input power $P_{in\,ELYZ}$. The following power balance stands:

$$P_{in\,ELYZ} = P_{stack} + P_{aux} \tag{28}$$

The auxiliary systems model is identical to the model used with the FC ($P_{aux} = P_{minaux} + k\,P_{stack}$). The net input power of the stack is computed using:

$$P_{stack} = \frac{P_{in\,ELYZ} - P_{auxmin}}{1 + k} \tag{29}$$

Fig. 8 shows a diagram of the input/output power on the ELYZ system.

Using the receptor sign convention and solving again for the current density in the quadratic equation obtained, the variation of the number of H2 moles in a time step Δt is obtained as:

$$\Delta n_{stack} = \frac{3600\Delta t}{4F}\left[-\frac{E_{ELYZ}}{R_{ELYZ}} + \sqrt{\frac{E_{ELYZ}^2}{R_{ELYZ}^2} + 4\frac{P_{stack}}{R_{ELYZ}S_{cell}N_{cell}}} \right] S_{cell}N_{cell} \tag{30}$$
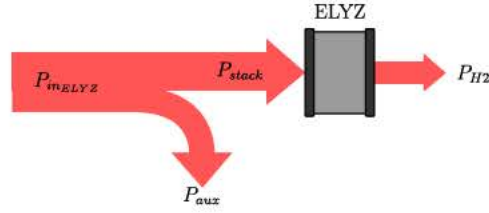
Fig. 8. Input/output ELYZ power flow.

Finally, the tank is modeled assuming the perfect gas law inside the H2 and O2 tanks. We consider that there is a 1/2 size ratio between H2 and O2 tanks, then $\Delta n_{O2} = \Delta n_{H2}/2$ et $V_{tank\,O2} = V_{tank\,H2}/2$. The pressures are however identical $p_{O2} = p_{H2}$. The pressure difference as a function of the variation in the number of moles is computed by:

$$\Delta p = \frac{\Delta n_{stack} RT}{V_{tank}} \tag{31}$$

From the variation of pressure the H2/O2 battery SOC is computed using:

$$SOC_{H2/O2}[k] = SOC_{H2/O2}[k-1] + \Delta t \frac{\Delta p[k]}{p_{tankmax}} \tag{32}$$

where $p_{tankmax}$ is the maximum tank pressure in bars.

Ageing model of the H2/O2 battery

The H2/O2 battery ageing model is based on a counter of the total operating hours and a constant degradation parameter of the stacks voltage given in μV/h. We consider that the FC end of life occurs when the stack voltage is 80% lower than the initial nominal voltage. As a complement, the ELYZ end of life occurs when the stack voltage is 120% higher than the initial nominal voltage. The calendar and operating SOH are computed using:

$$SOH_{cal}[k] = SOH_{cal}[k-1] - \frac{h_{op}}{\text{life span}} \tag{33}$$

$$SOH_{op}[k] = SOH_{op}[k-1] - \frac{h_{op}Coeff_{deg}}{0.2E_{stack100\%}} \tag{34}$$

where $Coeff_{deg}$ is -10 μV/h for the FC and $+10$ μV/h for the ELYZ, the calendar life span is 10,000 h for the FC and 26,000 h for the ELYZ, $E_{stack100\%}$ is the stack voltage at 100% SOH. The SOH is given by:

$$SOH = \min\left(SOH_{cal}, SOH_{fonct}\right) \tag{35}$$

The degraded voltage is computed at each time step for both the FC and ELYZ using:

$$\Delta E_{stack}[k] = Coeff_{deg} \times \Delta t \tag{36}$$

For the FC, the new stack voltage is given by:

$$E_{FC}^*[k] = E_{FC}^*[k-1] - \Delta E_{stack}[k] \tag{37}$$

The new SOC^* is computed by substituting E_{FC}^* in Eq. (26). With a degrading stack voltage the new SOH^* is actualized at each time step using:

$$SOH^*[k] = \frac{E_{PAC}^*}{E_{PAC}^{init}} \tag{38}$$

2.4. Economic model

The economical model considered is based on the annualized cash flow analysis using net present value (NPV) and the levelized cost of energy ($LCOE$). This modeling methodology is presented in detail in [27]. It has been widely

used in applications as in the software HOMER from NREL and in the literature for several techno-economical analysis with renewable energies in [14,4,2,20].

The NPV is a method used to analyze an investment taking account of the costs (negative cash flows) and revenues (positives cash flows) over a complete analysis period. It is defined for a present moment for cash flows obtained over N years, this is:

$$NPV = \sum_{n=0}^{N} \frac{F_n}{(1 + d_n)^n} \tag{39}$$

where F_n is the total cash flow for each annuity n, d_n is the nominal discount rate and N is the total number of annuities. The initial investment is accounted as a negative cash flow for year zero ($F_0 = -$Initial investment). For each annuity from $n = 1, \dots, N$ we compute the following coefficients:

$$COEFF_e = (1 + e)^n \tag{40}$$

$$PVIF_n = \frac{1}{(1 + d_n)^n} \tag{41}$$

where e is the mean annual inflation rate. The present value of the replacement cost of a storage equipment is obtained using:

$$PVreplcost_{Sto} = \frac{replcost_{Sto} \times invt_{Sto}}{(1 + d_n)^r} \tag{42}$$

where r is the year of replacement. Then the equipment depreciation D_n is estimated using the mixed depreciation law proposed in [27]. With D_n a new value of the equipment net book value is estimated for annuity n using:

$$netBookVal_n = netBookVal_{n-1} - D_n \tag{43}$$

The annual revenues Rev_n adjusted for the period inflation rate may be computed using the energy effectively injected to the grid E_{grid} (in MWh) and the feed-in-tariff FIT (in EUR/MWh):

$$Rev_n = E_{grid} \times FIT \times COEFF_e \tag{44}$$

Then the net taxable income $netTaxIn_n$, the tax on total income $InTax_n$ and the resulting after tax cash $afterTaxCash_n$ are obtained with:

$$netTaxIn_n = Rev_n - \cdots$$
$$\dots - OMcost_{tot} \times COEFF_e - D_n \tag{45}$$
$$InTax_n = TaxRate \times netTaxIn_n \tag{46}$$
$$afterTaxCash_n = Rev_n - \cdots$$
$$\dots - OMcost_{tot} \times COEFF_e - fedInTax_n \tag{47}$$

Finally, the NPV for each annuity NPV_n, its cumulated value and the global NPV for the total analysis period are computed using:

$$NPV_n = afterTaxCash_n \times PVIF_n \tag{48}$$
$$NPVcumul_n = NPVcumul_{n-1} + NPV_n \tag{49}$$
$$NPV = NPVcumul_n - invt_{tot} \tag{50}$$

The $LCOE$ is finally obtained with an iterative method for varying values of FIT. The $LCOE$ is obtained for the FIT value that yields the ratio $NPV/invt_{tot} = 0$ at the end of the analysis period.

3. Energy management strategy

3.1. Ancillary services

Many different power delivery services may be defined for this type of power producer in island grids. In this work, we will focus on two main "ancillary services":

- Day-ahead commitment with power production smoothing: a power commitment is defined as a discrete 30-min constant power profile that is generally obtained from a production forecast profile. This commitment should be respected inside a tolerance layer of 25% of the nominal installed power for the first year of operation, 20% for the second year and 15% from the third year and to the end of the delivery agreement.
- Primary energy reserve: a second service considered is a power reserve of 10% the nominal installed power that may be demanded one time per day during 15 min. This active power reserve is designed by the utility operator to achieve efficient control of the power grid area frequency.

The energy management block is presented in the following section but it may be composed of any desired management strategy from heuristic rule-based to optimal control strategies. The simulation is a power balance of the power produced by the RES and the power charged/discharged by the storage devices at the plant power delivery point and for each time step Δt. The inputs of the energy management block are the power production P_{prod} and commitment P_{eng} for the present time step k and the system states (notably the storage SOC) for the previous time step $k-1$. The outputs are the power reference for storage devices P_{sto}^{REF} and a power reference for production degradation P_{prod}^{REF} for the special cases with excess produced energy that cannot be charged by the storage devices (production with MPPT degradation). These power references are directly the inputs for the physical system simulation block. After the simulation of the power balance at the delivery bus, the output of this second block is the power injected to the grid P_{grid}, the wasted power due to MPPT degradation P_{wasted} and the power not-supplied during a violation of the day-ahead commitment $P_{notsupplied}$.

The violation of the day-ahead commitment is defined as a "commitment failure" (CF) and is computed using:

$$CF(\%) = 100\% \times \frac{1}{N} \sum_{k=1}^{N} CF(k) \tag{51}$$

where $CF(k)$ is a counter of a lower bound violation of the tolerance layer at each time step. This definition is quite similar to the variable Loss of Power Supply Probability (LPSP) thoroughly found in the literature. During a CF, the day-ahead commitment is not respected as a consequence of a low production output, an insufficient stored energy or a technical failure. A high bound violation of the tolerance layer is not considered as a system failure as it can be corrected with a MPPT degradation. A CF is accounted during a lower bound violation of the tolerance layer (for 1 min average power metering) and for a period of 10 min after the grid injected power is again inside the tolerance layer. The power delivered during a CF is not paid by the utility operator.

3.2. Heuristic energy management

The energy management strategy presented in this article is a basic rule-based algorithm designed with a certain trade-off margin between a good tracking of the day-ahead commitment and an efficient use of the storage device for an enhanced lifespan. The strategy is based on the position of the actual power production P_{prod} as a function of the tolerance layer. The energy management problem is then divided into three regions:

- If $P_{prod} > P_{eng} + tol$: this is a situation where an excess of produced energy may occur. In this case we define a desired power level to be delivered to the grid, we call this the goal power P_{goal} fixed in this case at upper bound of the tolerance layer $P_{goal} = P_{eng} + tol$. The storage power reference is defined as: $P_{sto}^{REF} = P_{goal} - P_{prod}$. If the battery is no longer able to absorb this excess power (reaching the maximum battery SOC or nominal power limitation) then the producer MPPT is degraded.
- If $P_{prod} < P_{eng} - tol$: this is a situation where a lack of produced energy may occur. In this case the desired goal power is fixed at the lower bound of the tolerance layer $P_{goal} = P_{eng} - tol$. The storage power reference is defined as: $P_{sto}^{REF} = P_{goal} - P_{prod}$. If the battery is no longer able to provide the needed power then a $CF(k) = 1$ is accounted.
- If $P_{eng} - tol \leq P_{prod} \leq P_{eng} + tol$: the power production is inside the tolerance layer. The storage is used only if $P_{eng} - P_{prod} < 0$ and $SOC < threshold$ (with the threshold defined in this case at 60%). If the condition holds, then the power reference for the storage is $P_{sto}^{REF} = P_{goal} - P_{prod}$ with $P_{goal} = P_{eng}$. Otherwise $P_{sto}^{REF} = 0$ and $P_{goal} = P_{prod}$.
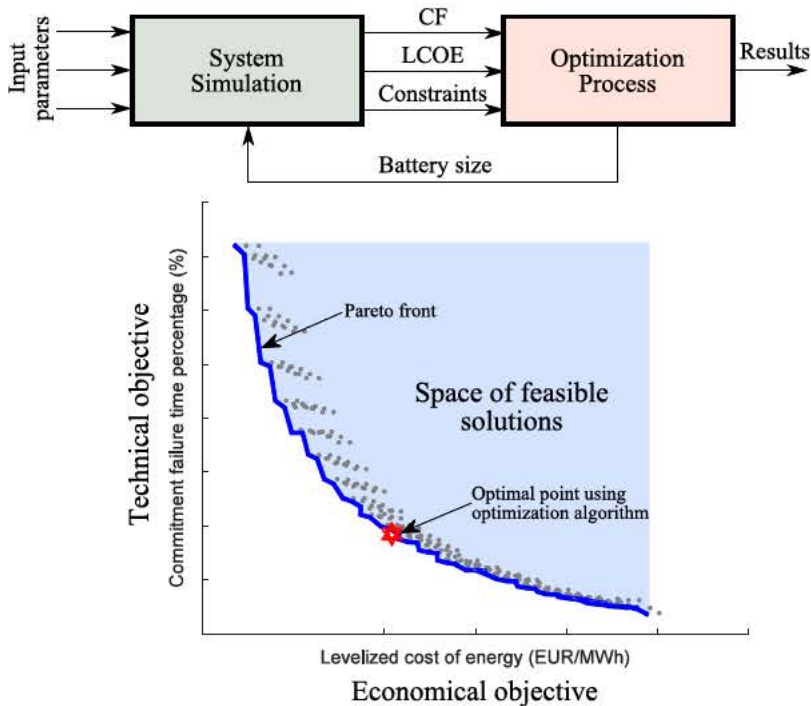
Fig. 9. Bi-objective optimization and Pareto optimal front.

4. Optimization results

In this section we present the results obtained for the techno-economical optimization of the hybrid power plant. Fig. 9 shows the definition of the multi-objective optimization problem and the solution using Pareto optimality. In this case, the bi-objective optimization function is composed of the commitment failure CF and the levelized cost of energy $LCOE$.

An analysis period of 15 years is fixed. The time step used for simulations is $\Delta t = 10$ min. The total wind power installed is 8 MW. The step-up transformer has 2350 kVA, 20 kV at 50 Hz. Additional losses for the battery conversion chain (inverter, cable losses, etc.) are estimated at 5%. The battery SOC is limited at $SOC_{min} = 30\%$ and $SOC_{max} = 90\%$.

Fig. 10 shows the Pareto optimal front obtained from variation of the Li-Ion battery size between 1 and 10 containers (580 kWh to 5.8 MWh). The simulation result for the case with no storage is included for comparison purposes. According to these results, a good techno-economical trade-off is obtained for battery sizes between 1 and 5 containers. The CF is lower than 4% and the $LCOE$ is between 130 and 160 EUR/MWh. These costs are comparable to those of Diesel engines power plants and are considerably lower than those of combustion turbine power plants. This is an interesting result in the context of island power systems.

Figs. 11 and 12 show the use of the simulation tool for sensitivity analysis with varying parameters on the production forecast and battery CAPEX values respectively. A varying product factor between -5% and -10% is applied to the forecast value and a $\pm 30\%$ product factor on the battery CAPEX. The factor on the day-ahead forecast, used to define the delivered power commitment, has a stronger impact on the CF technical indicator, whereas a $\pm 30\%$ variation on the battery CAPEX has an impact on both the technical and economical objectives.

A series of results is obtained for simulations with a fixed battery size of 3 containers (3×580 kWh). The results are presented in Figs. 13–15. For this 15 year simulation, the battery reaches the end of the analysis period at $SOH = 31\%$, without any battery replacement. A $CF = 2.5\%$ and a $LCOE = 136.7$ EUR/MWh are obtained. Fig. 13 is an extract of one week of simulation showing the different system powers and the associated evolution of the battery SOC. Given that the FIT value exceeds 200 EUR/MWh, the payback period of the whole plant is
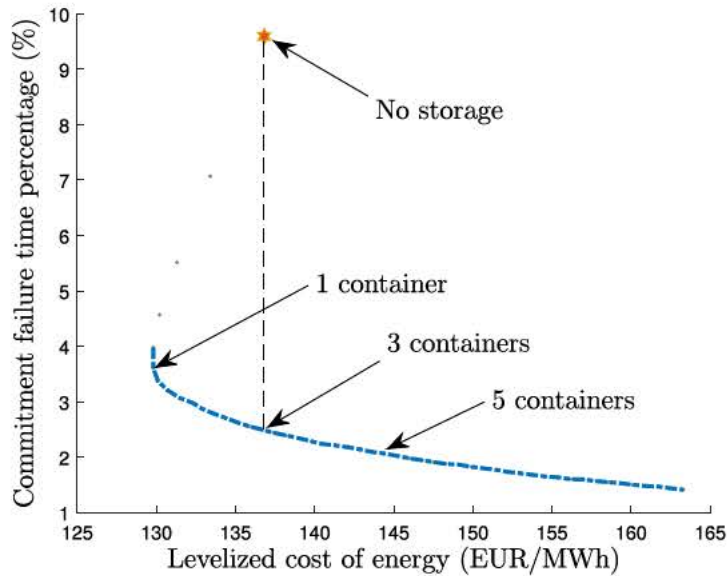
Fig. 10. Pareto optimal front for Wind farm with Li-Ion battery.
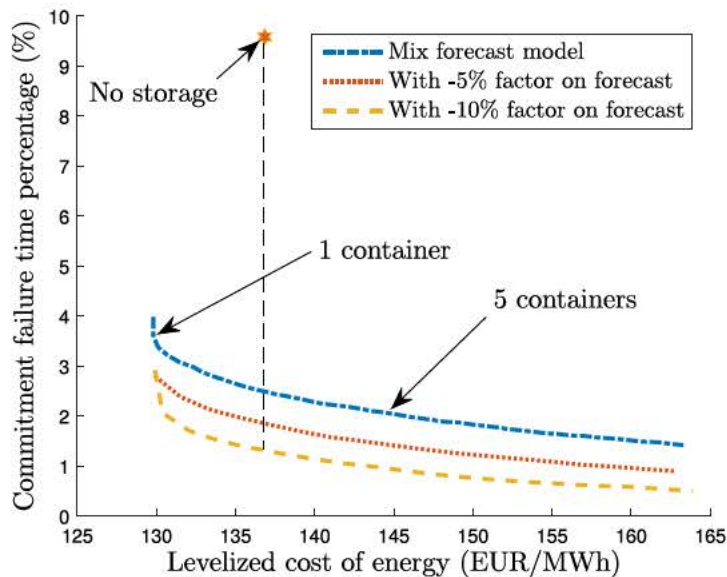

Fig. 11. Pareto optimal front with varying factor on production forecast.

approximatively 8 years. Please note that these calculations have been made on standard CAPEX/OPEX figures and have not taken into account extra costs implied by the local context: insurance costs in a hurricane zone, transportation costs for cranes for installation and maintenance, local taxes, etc. This can explain the difference between our calculated $LCOE$ and the FIT.

A Pareto optimal front comparison between WT+Li-Ion, WT+H2/O2 and WT+Li-Ion+H2/O2 is presented in Fig. 16. It is interesting to note the improvement of the techno-economical performance of the hybrid storage option Li-Ion+H2/O2 when compared with only H2/O2 storage. However, the Li-Ion-only option is still (under the supposed set of input parameters) the best techno-economical solution. Despite these results, H2 storage remains a promising environmental friendly option for the near future. Some factors may influence the insertion of this type of storage in
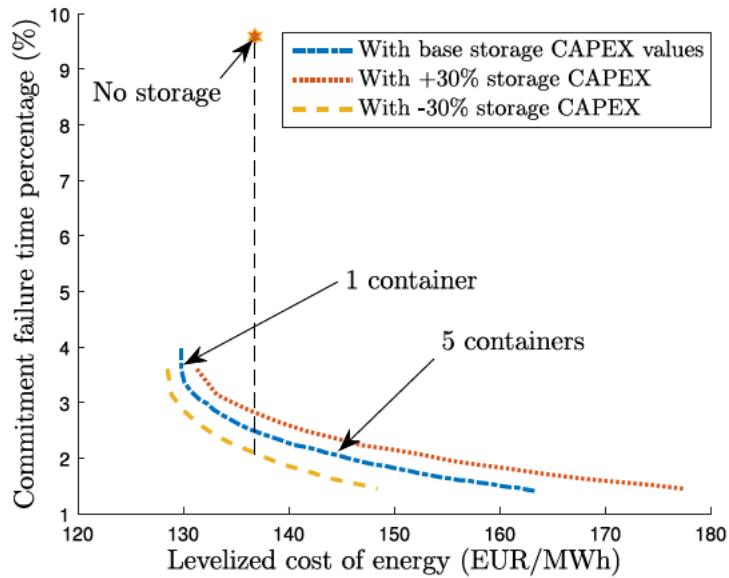
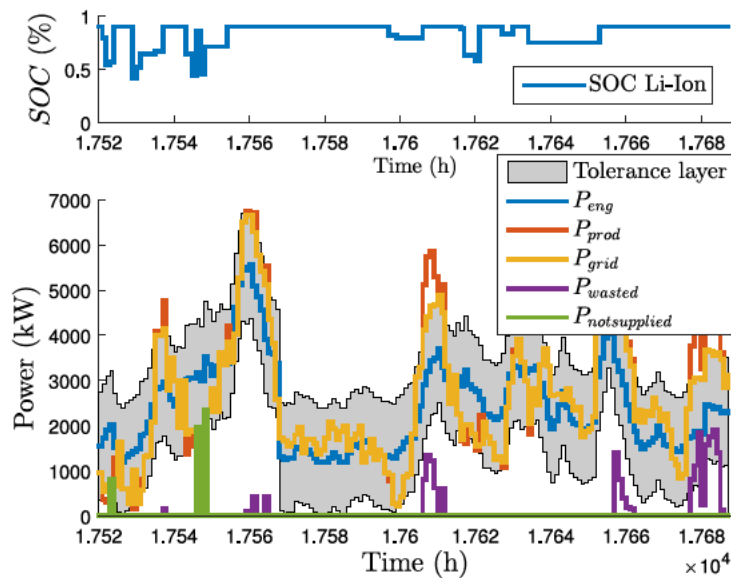Fig. 12. Pareto optimal front with varying factor on battery CAPEX.

Fig. 13. Simulation results WT+Li-Ion: system powers for the first week of the third year.

the future: reduction of CAPEX for the complete H2/O2 solution, a secondary applicative use of the thermal energy resulted from energy conversion, or even the implementation of an optimized energy management strategy involving this type of storage.

5. Conclusions

In this article a modeling tool for techno-economical storage sizing is presented. The studied system is a hybrid power plant composed of a wind farm, li-ion and/or H2/O2 batteries in the context of an island power grid. The sizing
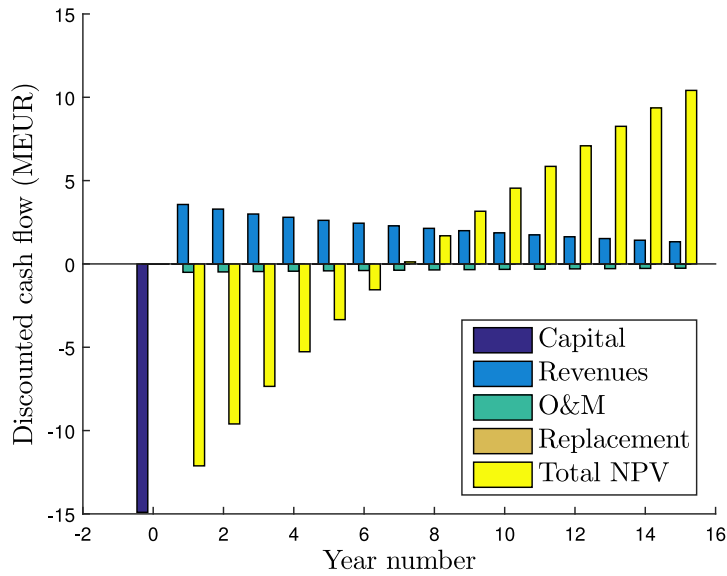
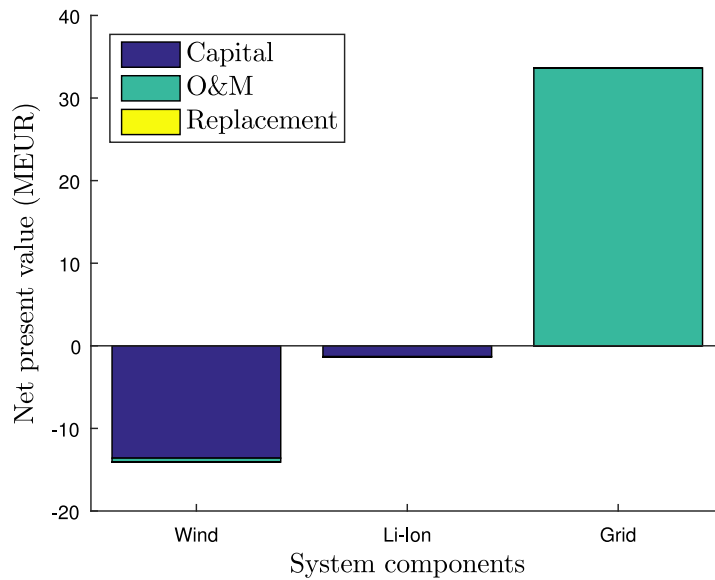**Fig. 14.** Simulation results WT+Li-Ion: cash flow and NPC progress.

Fig. 15. Simulation results WT+Li-Ion: system costs by component.

results and the plant costs obtained are promising in the insular context and in comparison with other traditional power plant technologies. The modeling tool includes ageing models of the storage devices. This modeling tool is suitable for decision making in planning stages. Complete sensitivity studies may be conducted with this type of tool, with some examples presented in this article. The modeling tool has been completed with other RES sources such as PV. The obtained results show a clear advantage for a hybrid system with only Li-Ion batteries, despite a promising future for the complete hybrid option including H2/O2 storage. Other future works may involve a complete sensitivity study of varying parameters and towards the implementation of an optimized energy management strategy.
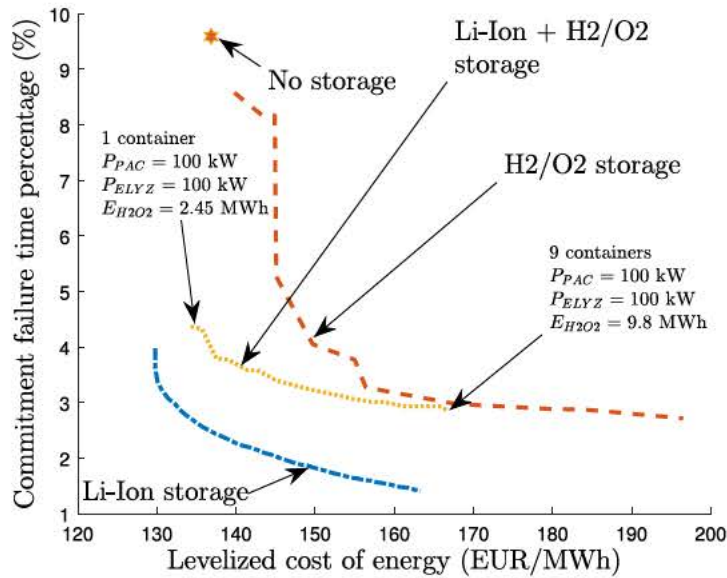
Fig. 16. Pareto optimal front comparison between: WT+Li-Ion, WT+H2/O2 and WT+Li-Ion+H2/O2.

References

[1] C.R. Akli, B. Sareni, X. Roboam, A. Jeunesse, Integrated optimal design of a hybrid locomotive with multiobjective genetic algorithms, IJAEM 3/4 (30) (2009) 151–162.

[2] J.L. Bernal-Agustin, R. Dufo-Lopez, Economical and environmental analysis of grid connected photovoltaic systems in Spain, Renew. Energy 31 (2006) 1107–1128.

[3] H. Bludszuweit, J.A. Dominguez-Navarro, A probabilistic method for energy storage sizing based on wind power forecast uncertainty, IEEE Trans. Power Syst. 26 (3) (2011) 1651–1658.

[4] L. Bridier, D. Hernandez-Torres, M. David, P. Lauret, A heuristic approach for optimal sizing of ESS coupled with intermittent renewable sources systems, Renew. Energy 91 (2016) 155–165.

[5] M. Chowdhury, M. Rao, Y. Zhao, T. Javidi, A. Goldsmith, Benefits of storage control for WPP in power markets, IEEE Trans. Sust. Energy 7 (4) (2016) 1492–1505.

[6] A.S. de Ibarra, A. Milo, H. Gaztanaga, V. Debusschere, S. Bacha, Co-optimization of storage system sizing and control strategy for intelligent PV power plants market integration, IEEE Trans. Sust. Energy 7 (4) (2016) 1749–1761.

[7] F. Gailly, Alimentation électrique d'un site isolé à partir d'un générateur photovoltaïque associé à un tandem électrolyseur/pile à combustible (batterie H2/O2), (Ph.D. dissertation), Université de Toulouse, 2011 (in French).

[8] P. Garcia, J.P. Torreglosa, L.M. Fernández, F. Jurado, Improving long-term operation of power sources in off-grid hybrid systems based on RE, H2 and battery, J. Power Sources 265 (2014) 149–159.

[9] F. Garcia-Torres, C. Bordons, Optimal economical schedule of hydrogen-based microgrids with hybrid storage using model predictive control, IEEE Trans. Ind. Electron. 265 (2014) 149–159.

[10] B. Guinot, Y. Bultel, F. Montignac, D. Riu, I. Noirot-Le Borgne, Economic impact of performances degradation on the competitiveness of energy storage technologies (Part 1), Int. J. Hydrog. Energy 38 (2013) 15219–15232.

[11] P. Haessig, B. Multon, H.B. Ahmed, S. Lascaud, P. Bondon, Energy storage sizing for wind power: impact of the autocorrelation of day-ahead forecast errors, Wind Energy 18 (1) (2015) 43–57.

[12] P. Harsha, M. Dahleh, Optimal management and sizing of energy storage under dynamic pricing for the efficient integration of renewable energy, IEEE Trans. Power Syst. 30 (3) (2015) 1164–1181.

[13] D. Hernandez-Torres, C. Turpin, X. Roboam, B. Sareni, Modélisation en flux d'énergie d'une batterie Li-Ion en vue d'une optimisation technico économique d'un micro-réseau intelligent, in: Symposium de Genie Electrique, 2016 (in French).

[14] D. Hernandez-Torres, L. Bridier, M. David, P. Lauret, T. Ardiale, Technico-economical analysis of a hybrid wave power-air compression storage system, Renew. Energy 74 (2015) 708–717.

[15] F. Kazhamiaka, C. Rosenberg, S. Keshav, Practical strategies for storage operation in energy systems: Design and evaluation, IEEE Trans. Sust. Energy 7 (4) (2016) 1602–1610.

[16] R. Khodabakhsh, S. Sirouspour, Optimal control of energy storage in a microgrid by minimizing conditional value-at-risk, IEEE Trans. Sust. Energy 7 (3) (2016) 1264–1273.

[17] T. Lambert, P. Gilman, P. Lilienthal, Micropower System Modeling With HOMER, John Wiley & Sons, Inc., 2006.

[18] N.A. Luu, Q.T. Tran, S. Bacha, V.L. Nguyen, Optimal sizing of a grid-connected microgrid, in: 2015 IEEE Inter. Conf. on Ind. Tech., ICIT, pp. 2869–2874.

[19] E. Nasrolahpour, S.J. Kazempour, H. Zareipour, W.D. Rosehart, Strategic sizing of energy storage facilities in electricity markets, IEEE Trans. Sust. Energy 7 (4) (2016) 1462–1472.

[20] M. O'Connor, T. Lewis, G. Dalton, Techno-economic performance of the pelamis P1 and wavestar at different ratings and various locations in Europe, Renew. Energy 50 (2013) 889–900.

[21] P. Pinson, G. Papaefthymiou, B. Klockl, J. Verboomen, Dynamic sizing of energy storage for hedging wind power forecast uncertainty, in: Proceedings of the IEEE PES General Meeting 2009.

[22] D. Prichard, J. Theiler, Generating surrogate data for time series with several simultaneously measured variables, Phys. Rev. Lett. 73 (17) (1994) 951–954.

[23] Y. Riffonneau, S. Bacha, F. Barruel, S. Ploix, Opt. PF management for grid connected PV systems with batteries, IEEE Trans. Sust. Energy 2 (3) (2011) 309–320.

[24] R. Rigo-Mariani, B. Sareni, X. Roboam, A fast optimization strategy for power dispatching in a microgrid with storage, in: IECON 2013, pp. 7902–7907.

[25] Y. Ru, J. Kleissl, S. Martinez, Storage size determination for grid-connected photovoltaic systems, IEEE Trans. Sust. Energy 4 (1) (2013) 68–81.

[26] SAFT, Lithium-Ion Battery Life: Solar Photovoltaics (PV) - Energy Storage Systems (ESS), Technical Report Document No. 21893-20514, SAFT, 2014.

[27] W. Short, D.J. Packey, T. Holt, A Manual for the Economic Evaluation of Energy Efficiency and Renewable Energy Technologies, Technical Report NREL/TP-462-5173, National Renewable Energy Laboratory, 1995.

[28] O. Tremblay, L.A. Dessaint, Experimental validation of a battery dynamic model for EV applications, World Electric Vehicle J. 3 (2009).